

Thin 10–100 nm film in contact with substrate: Dynamics after femtosecond laser irradiation

This content has been downloaded from IOPscience. Please scroll down to see the full text.

2015 J. Phys.: Conf. Ser. 653 012003

(<http://iopscience.iop.org/1742-6596/653/1/012003>)

View [the table of contents for this issue](#), or go to the [journal homepage](#) for more

Download details:

IP Address: 95.25.84.93

This content was downloaded on 11/11/2015 at 16:58

Please note that [terms and conditions apply](#).

Thin 10–100 nm film in contact with substrate: Dynamics after femtosecond laser irradiation

V A Khokhlov¹, N A Inogamov¹, V V Zhakhovsky², V V Shepelev³
and D K Il'nitsky²

¹ Landau Institute for Theoretical Physics of the Russian Academy of Sciences, Akademika Semenova 1a, Chernogolovka, Moscow Region 142432, Russia

² All-Russia Scientific Research Institute of Automatics, Sushchevskaya 22, Moscow 127055, Russia

³ Institute for Computer-Aided Design of the Russian Academy of Sciences, Vtoraya Brestskaya 19/18, Moscow 123056, Russia

E-mail: vadim.aries@gmail.com

Abstract. Femtosecond laser irradiation of a thin gold film deposited on the thick glass substrate is considered. The thickness of a film has the order of a few microns and focal spot is small. Underlying physics of processes after irradiation is studied with combined approach of two-temperature hydrodynamic and MD simulations. Found are two adsorbed fluence thresholds $F_s < F_a$ and three regimes of motion, in comparison with the freestanding film. There is oscillatory mode when the film oscillates remaining on substrate for $0 < F < F_s$. For $F_s < F < F_a$ the film breaks away from substrate because negative pressure overcomes the cohesion strength of the film-substrate contact. For $F_a < F$ there is inner disruption of the film happened before the separation of metal from dielectric substrate.

1. Introduction

Ultrashort laser pulse may induce the interesting combinations of thermal and hydrodynamic phenomena including foaming and freezing of molten metals and semiconductors [1–3] formation of chaotic surface nanostructures and mesoporous layers [1–3], and superelastic shocks [4, 5]. Appearance of negative pressures within the frontal surface layer heated by a laser has a key importance for understanding of frontal nucleation, foaming, and spallation often called ablation (mass removal) in laser community. Release and movement of spallation shell allows understanding the puzzle of Newton rings [6, 7]. Disruption of a free-standing plane film quickly heated by a laser is the simplest model of laser spallation [8–14] in which the sharp spallation (ablation) threshold F_a determines dynamics of the free-standing film. Problem of significant importance is: how this picture will change if the film is deposited onto substrate? This problem is solved in the report. It is found that now there are two thresholds $F_s < F_a$ and three regimes of motion in comparison with the freestanding film. For $0 < F < F_s$ the film oscillates remaining on substrate. Oscillations decay in time due to emission of acoustic waves into substrate. For $F_s < F < F_a$ the film breaks away from substrate because negative pressure propagating with acoustic waves arrives to a film-substrate contact and overcomes the cohesion strength of the contact. In the third regime $F_a < F$ there is inner disruption of the film happened before a moment when negative pressure separates metal and dielectric substrate at the contact.



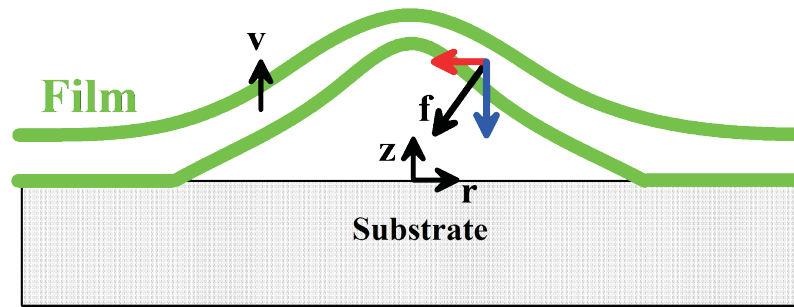


Figure 1. Scheme of peeling and detachment of the film on the substrate.

2. Small spots, peeling the film from the substrate and the formation of the dome

Consider the impact of a femtosecond laser pulse on a thin gold film deposited on the thick glass substrate with the thickness of the order of a few microns. Focal spot is small enough $R_L \sim \lambda$, and the film thickness is comparable to the thickness of the layer of warm $d_f < d_T$, where R_L , λ , d_T being the radius of the focal spot, the wavelength and the thickness of warming consequently.

Figure 1 shows the overall picture of detachment of the film from the substrate and forming a dome-shaped swelling of the film. In the experiments [15–17] using gold film thickness of 10–100 nm. This film was coated with a thick (many microns) glass substrate. The laser illuminates the film through the air from the top or through the bottom of the glass. The direction of arrival of the heating beam does not matter. That is because the film is uniformly warmed during the time less than one picosecond due to the large electron thermal conductivity of gold on the two-temperature stage. This time is short in comparison with the characteristic acoustic time $t_s = d_f/c_s \sim 10$ ps.

The process of separation of the film from the substrate is allowed to consider in a one-dimensional formulation, when the variables depend only on the coordinate z and time t . We can do this due to the fact that the transverse scale R_L (see figure 1) has the order of a wavelength, i.e. order of a micron and the normal scale z has the order of the thickness of a film which is 10–100 times less. In the process the film separation velocity distribution $v(r)$ forms, with which the film loses its dynamic contact with the substrate. Velocity distribution is formed at the time of the order of the acoustic time scale $t_s \sim 10$ ps. The velocity v has the order of 10–100 m/s. Therefore, the formation of the dome with a height of about radius R_L occurs at large (compared to the t_s) times:

$$t_{dome} \sim R_L/v = (R_L/d_f)(1/M)t_s \gg t_s, \quad M = v/c_s.$$

Both factors in these estimates are large, so the formation of the dome is delayed by tens of nanoseconds.

Cooling of the dome on the dielectric substrate is mainly due to the transfer of heat by electron heat conduction along the film. Thermal losses in a poorly conductive dielectric substrate are small. Radiation losses can be neglected. A simple estimate of the cooling and recrystallization of the hot spots gives $t_{cool} \sim R_L^2/\chi \sim 10$ ns, where $R_L \sim 10^{-4}$ cm, $\chi = \kappa/c \sim 1$ cm²/t, χ – thermal diffusivity, κ , c – thermal conductivity and heat capacity of the metal.

As you can see, times of the dome formation and freezing have the same order. This fact is related to the formation of solid domes on the irradiated surface.

The film separation time is several orders less than the dome formation time. Therefore, the separation of the film can be considered separately. This approach greatly simplifies the calculations. Process of the peeling of a film is modeled with two-temperature hydrocode (2T-HD) below in section 3. Phase transitions and negative pressures in a film can be taken into account due to semiempirical wide-range equations of state [18–21].

3. The oscillations or detachment of the film from the glass substrate

Consider the dynamics of the film irradiated with an ultrashort pulse on the substrate. It turns out that, depending on the energy embedded in the film F_{abs} are three modes. They are separated by two thresholds F_s and F_a . Below the first threshold (threshold of the delamination) F_s film remains on the substrate. The magnitude of this threshold is determined by the strength of adhesion between the glass and the film. Between the thresholds F_s and F_a film is peeled from the glass. Actually, it peels off as a whole. Above the threshold F_a film is broken. Moreover, film breakdown occurs before the tensile stress wave reaches the glass-to-metal contact.

The problem of irradiation of loose film (which has two border with vacuum) was considered in many papers [8–13, 22], starting from [8]. In [13] the influence of the film thickness is analyzed. We are interested in thin films $d_f < d_T$ which are substantially uniformly heated prior to significant hydrodynamic motion. Why it is advisable to recall the expansion of a uniformly heated loose film? The fact that the acoustic impedance of gold is much greater than the acoustic impedance of the glass [23]. Impedance of vacuum is equal to zero. In this sense, the gold film on a glass similar to the loose film, but has a small asymmetry associated with the low impedance of the glass.

Loose film gives us a clear idea of the ablation threshold F_a , on which the film is torn in half [8–10, 12, 13, 22]. In this case, the ablation threshold F_a is slightly higher than in the case of loose film as the rarefaction wave running from the contact of gold-glass is slightly weaker than in the case of loose film. The attenuation of this wave dilution occurs because there is a small but not zero, the acoustic impedance of the glass.

Between the thresholds F_s and F_a final velocity of the center of mass of the film removing from the glass arises from the asymmetry problem. In the symmetric case the velocity of the center of mass is equal to zero. Because of the smallness of the asymmetry the center of mass velocity is much smaller (times ratio of acoustic impedances, see [23]) than the velocity of oscillating loose film of equal thickness and equal adsorbed energy.

In this article first introduced a complete numerical solution of the problem of heating the film on the substrate. In [23] obtained a simplified analytical solution in the acoustic approximation mode and under condition of $F_s < F_{abs} < F_a$. Also important is that the oscillatory mode $F_{abs} < F_s$ and with an internal film-break mode $F_{abs} > F_a$ are described.

3.1. Oscillatory mode

On figures 2-4 are shown damped oscillations of the gold film observed in energy investments below the delamination of the film from the glass: $F_{abs} < F_s$. Contact with the vacuum on the left. The instantaneous position of the right contact gold-glass easily identified by the fracture pressure profile, which is discontinuous pressure gradient. The jump is due to a large difference in density of the glass (2.23 g/cm^3) and gold (19.3 g/cm^3). The pressure in the glass is substantially less than the pressure in gold, as the acoustic impedance of the glass $z_g = \rho_g c_g = 0.87 \cdot 10^6 \text{ (g/cm}^2\text{)}$ is small in comparison to the acoustic impedance of gold $z_{Au} = \rho_{Au} c_{Au} = 5.9 \cdot 10^6 \text{ (g/cm}^2\text{)}$. Impedance ratio of the gold to the glass is equal to $q = 6.8$.

The emergence of the movement shown on figures 2-4 is due to the rapid heating of the film. The heating time of the electron subsystem of the whole film has the order of a small amount of the order of one picosecond. This time is short compared to the acoustic scale. Therefore, in essence there is a “blow” to the film. In fact, on the borders of the film with a vacuum and the glass there is a situation with the collapse of the release of pressure as the pressure in the metal increases rapidly for 1 ps, and decay occurs on an acoustic time scale, which has the greater order of magnitude.

Accordingly, fluctuation of the film shown on figures 3 and 4 are far from sinusoidal oscillations. They have sharp corners, which are followed by a rapid increase of pressure in the left and right borders of the film. The sharp pressure rise in figure 4 at time points $t = 0, 40, 80$

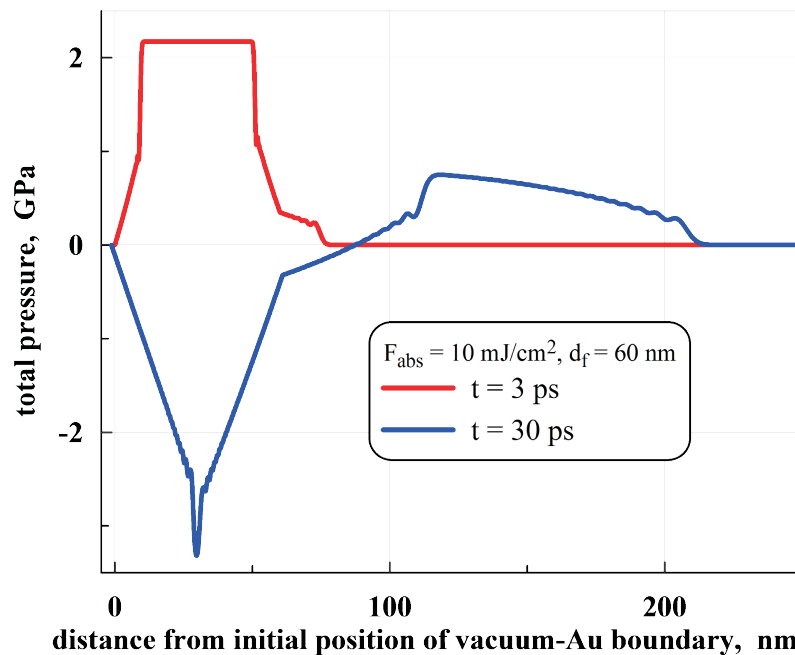


Figure 2. Pressure profiles in a film of gold and glass at times moments of 3 and 30 ps.

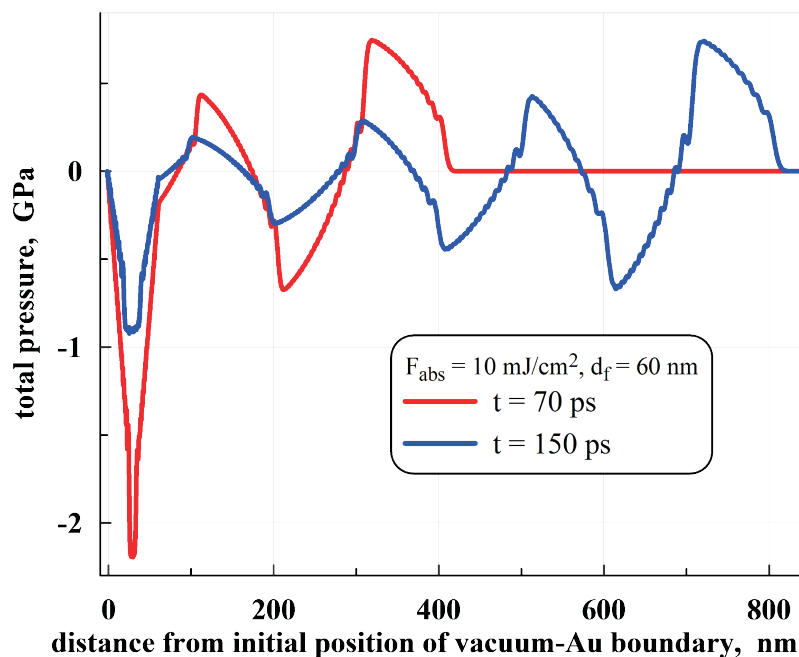


Figure 3. Oscillating film emits acoustic waves in the glass. It is seen as a gradual fluctuation of the oscillation wave train is formed, stretching out into the glass. Gradually, the oscillation amplitude decreases due to radiation losses.

and 120 ps etc. is generated by the rapid heating of the left border (border with vacuum).

Moreover, figure 7 shows the pressure on the *right* border (border with glass). Speed of response (at $t \approx 0$) on the *right* border to the *left* border of the heating characterizes the rate of heat flow through the film.

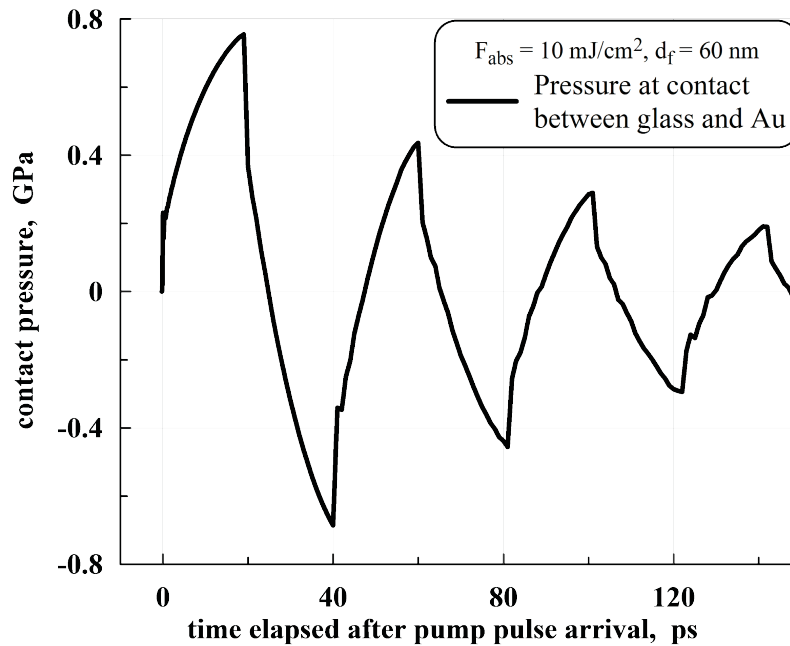


Figure 4. Damped oscillations of the pressure at the contact between gold and glass.

Sudden pressure drop times of about 20, 60, 100 and 140 ps in figure 4 characteristics are caused by the arrival of the head of the rarefaction wave from the left border (vacuum) on the right boundary (glass). In its first arrival this expansion wave brings information about the existence of the border with the vacuum in the thickness of the gold film and the glass.

Note that if the distribution of the heat wave in two-temperature metal occurs rapidly, the two-temperature relaxation in gold is rather high and amounts to 10–15 ps. This is due to the large mass of gold ions, because of which the ion exchange electron energy slows down. Thus, the relaxation time has the order of sound time $t_s = d_f/c_s$. During the relaxation the total pressure changed from a predominantly electronic pressure (at the initial stage of the two-temperature phase) to preferably ionic pressure (after a two-temperature step). This fact changes the Gruneisen parameter, which for the ionic subsystem is about twice larger than that of the electron subsystem [24]. Since the internal energy stored in the film varies little during electron-ion relaxation, this increase Gruneisen parameter leads to an increase in the total pressure during relaxation. This fact affects the wave profile.

3.2. Delamination of the film

In the range of the absorbed fluence $F_s < F_{abs} < F_a$ holds a mechanical detachment of the film from the substrate. The voltage between the cohesion metal and the dielectric substrate is determined by the surface energy of their interaction. Cohesion tensions p_{coh} are in the range from zero to about one GPa. The exact values are poorly known. Outside the vicinity of the threshold delamination, p_{coh} variation in the range of 0–1 GPa pretty little effects the velocity of the center of mass v of the separated film. That's because at the stage the increase of the velocity of the center of mass v takes place, the value of contact pressure is more than the value of p_{coh} . Furthermore, the duration of step a positive pressure is greater than the length of time in which a contact pressure becomes negative and $-p_{coh}$ reaches the end of this time. We return to this issue below. Now let's proceed to figure 5.

Figure 5 shows the distribution of expansion waves from the edges of the film to the center and beyond. At the time of 3 ps rarefaction waves are about 10 nm (initial film thickness

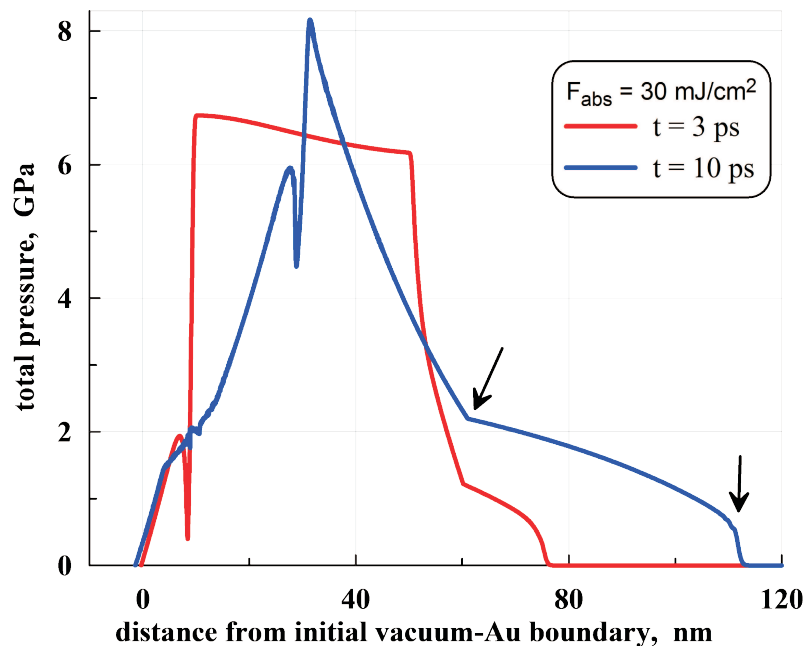


Figure 5. Rapid rise in pressure in the film and the movement of expansion waves from contact with the vacuum on the left and right with the glass in the thickness of the film. Arrows indicate the position of the contact and the shock at the time of 10 ps.

of 60 nm). Rarefaction wave consists of a sharp jump in and smoother plot behind it. On the left can be seen the failure of the rarefaction wave, the appearance of which is caused by an extremely sharp increase in the electron pressure in the skin layer of gold in a very short duration ($\tau_L = 100$ fs) laser pulse. This very sharp increase in the electron temperature and electron pressure associated with irradiated left border (border with vacuum). Right on the border there is no increase. Width of the dip is small, and it has the order of ~ 0.3 nm. This distance is comparable to the average interatomic distance. Therefore, it is not seen in MD simulations.

By the time of 10 ps, the left and right of the rarefaction wave both are spread to the distances about 30 nm, and they meet in the center of the film. See figure 5. Then left wave proceeds to the right, and right wave proceeds to left. The amplitude of the pressure in the center begins to decline sharply, see figure 6. Compare the two simulations with different values of F_{abs} on figures 2 and 5 at the time of 3 ps. Pressure increased approximately in direct proportion to the input energy F_{abs} . In addition, we see that the pressure outside the pressure drop grows with time during the two-temperature stage due to the arrival of expansion waves from the edges of the film. Compare the maximums of pressure on figure 5 at times of 3 ps and 10 ps. Increase of pressure is caused by the overflow of energy from a “soft” (with less Grüneisen parameter) electron gas in a rigid ion subsystem. The ratio of the electron and ion internal energy changes during the two-temperature relaxation, and the total internal energy of the film remains approximately constant (losses due to the transition to the kinetic energy of the gold and the kinetic and internal energy of the glass are small).

Glass pressure is substantially less than the maximum positive and negative (in absolute value) the pressure in the film. The provisions of the shock wave in the glass are indicated by arrows on figure 6. At the selected input energy F_{abs} hydrodynamic velocity is much smaller than the speed of sound – compare the distances traversed by the shock wave (two arrows to the right on figure 5) and the shift of the pressure profile on the left (near the origin) on figure

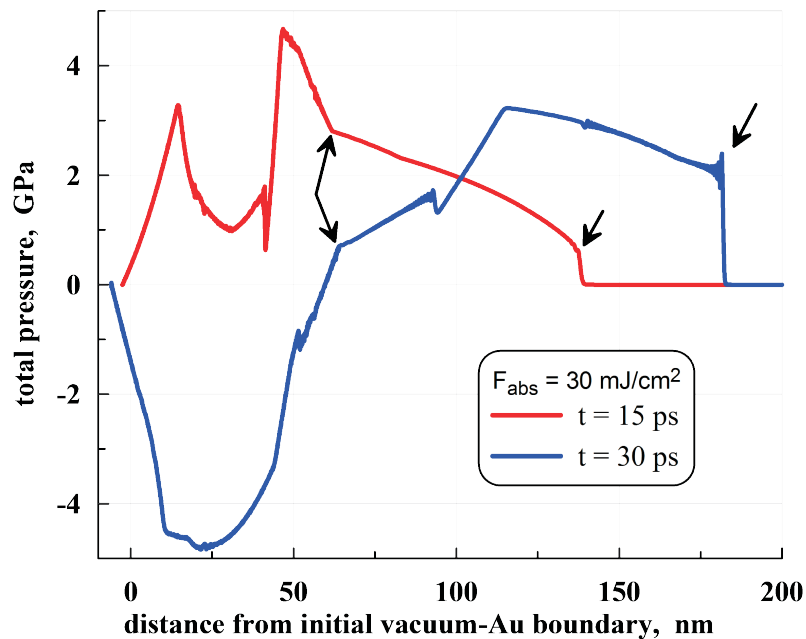


Figure 6. The situation after the passage of the head characteristics rarefaction waves through each other when the pressure in the central region of the film begins to decline rapidly.

5. Note that the temperature of gold at the end of a two-temperature phase is about 1800 K. The film is completely melted.

At the time of 30 ps contact pressure on the gold-glass is still positive, see figure 6. The double arrow shows how the reduced contact pressure on the time interval 15–30 ps. In the calculation shown on figure 5-7 the cohesion tension p_{coh} is equal to 1 GPa. The pressure is reduced on contact, then it crosses the zero point, then it approaches and crosses the threshold of -1 GPa. The film is separated from the substrate when the tensile stress at the contact reaches p_{coh} .

On figure 7 are illustrated two time moments – before and after the intersection of the contact pressure threshold p_{coh} , which is adopted for the value -1 GPa. At a time when declining pressure on the contact value crosses p_{coh} , the pressure on the right border of gold and glass in the left margin abruptly vanish. At this time, the gold-glass contact is broken in the sense that there is a gap between the edges of the gold and glass. Vapor pressure in the gap can be neglected in comparison to background stress ~ 1 GPa $= 10^4$ atm in the condensed phase. Therefore in the gap at its ends the pressure is zero. The gap is slowly expanding, and in gold (left) and glass (right) spallation impulses run. Distribution of spallation pulse and expansion of the gap are shown on figure 8. Impulses run with the speed of sound in gold and glass, and the gap is expanding at the speed of ~ 100 – 150 m/s, which is small compared to the speed of sound.

The arrows on figure 8 at points 55 nm and 84 nm mark position of the front spall pulse respectively in gold and glass. In the glass the speed of sound is bigger, so the spall impulse runs a greater distance (they have the same start point and start time).

To the border of the glass on the right propagates the flow of characteristics that carries trivial information about the quiescent homogeneous glass, about which it was before impact. Since the gap at the interface after heating pressure is equal to zero, the reflected characteristics remain trivial. Therefore, for the spall pulse in the glass, the pressure (see figure 8) and speed (see figure 9) become equal to zero.

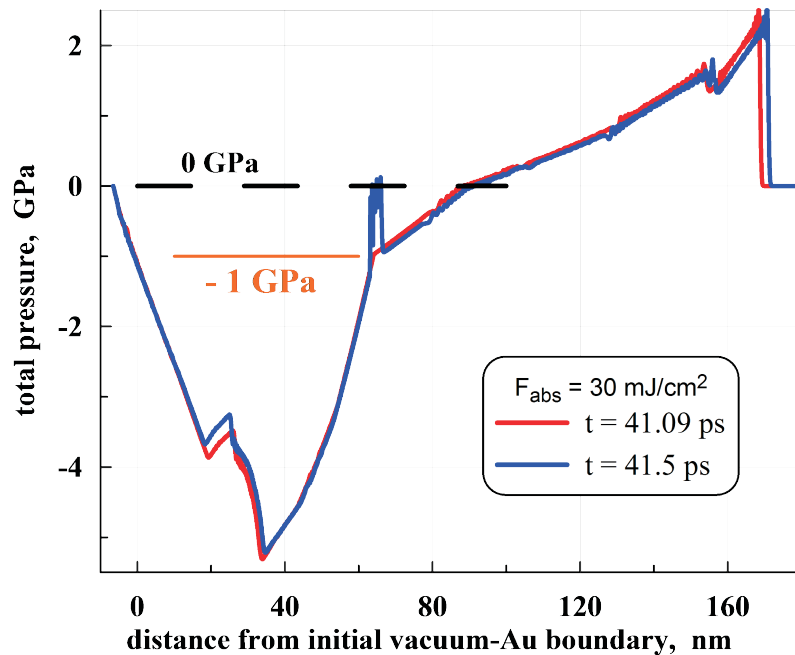


Figure 7. The evolution of the pressure profile in the vicinity of the time at which the film is separated from the glass. At the time of separation, the contact pressure on the gold-glass abruptly changes from -1 GPa to a value of 0.

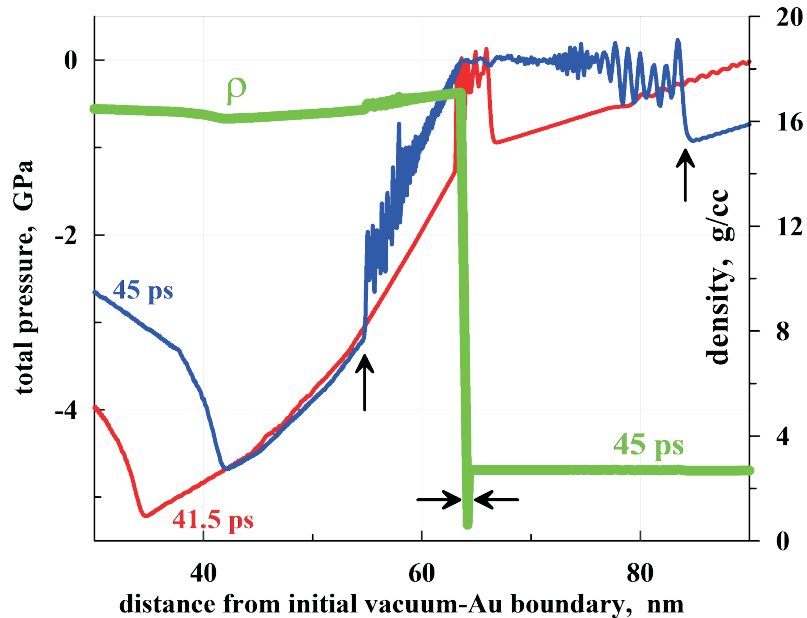


Figure 8. Radiation of weak shock waves (spall pulse) from the point of discontinuity of contact gold-glass at break of 41.10 ps. Arrows indicate the position of the shock wave at the time of 45 ps in gold and glass. Double arrow indicates the gap between the divergent edges of gold and glass at the time of 45 ps.

On the contrary, in gold to the boundary with glass propagates the flow of characteristics carrying non-trivial information. This flow is reflected from the free boundary (after breaking

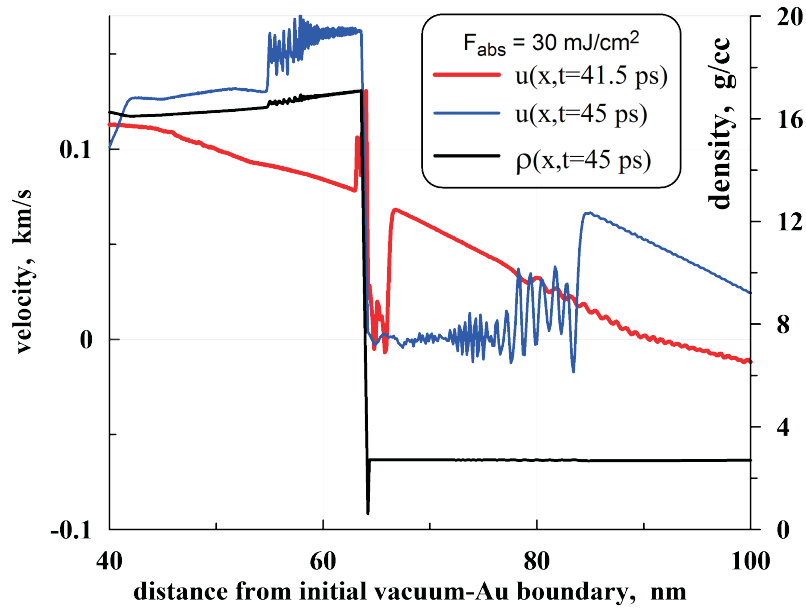


Figure 9. Velocity distribution and density in the vicinity of the broken glass gold contact.

the contact becomes a free boundary) with also non-trivial characteristics. Accordingly, for the spall pulse in gold neither tension nor speed is not equal to zero, see figure 8. On the figure 8 the path traversed by the spall momentum in gold as of 45 ps corresponds to the interval from the left arrow till the gap (the density jump gold-glass). Spall pulses in gold and glass at points of 41.5 ps and 45 ps are also clearly visible on figure 9. The distance behind glass spall pulse is greater because the speed of sound in the glass is several times greater than in the gold.

Cohesion tension is equal to 1 GPa. With a negative contact pressure of such amplitude the film rupture occurred at the time of 41.1 ps. Therefore, the amplitude of both spall pulse is also equal to 1 GPa, see figure 8.

3.3. The final velocity of the center of mass of the film after separation from the glass

This mode corresponds to the energy interval $F_s < F_{abs} < F_a$, when the film is separated from the substrate as a whole. Before and after the separation from the glass inside the film there is a non-trivial velocity distribution. The velocity is distributed heterogeneously and this distribution is unsteady – it arises as a result of the game left and right waves, running around the film. However, the velocity v of the center of mass of the film, of course, immediately ceases to vary immediately after detachment of the film. Variation of the speed of the center of mass follows the law:

$$v(t) = \frac{1}{\mu} \int_0^1 p(t_1) dt_1, \quad \mu = \int_1^2 \rho dz. \quad (1)$$

Here, under the first integral stands pressure on contact, or rather the pressure in gold on the border between gold and glass. This integral is divided by the weight of the film per unit area of the film. Limits 1 and 2 of the second integral are related to the borders of the film.

In the first half-period of the first oscillation on figure 4 contact pressure is positive, and the speed of the center of mass is increasing. In the second half-period at the contact pressure becomes negative and the speed of the center of mass is decreasing. In the vibrational mode where there is no separation of the film, the average speed of the film over time is zero.

Consider mode $F_s < F_{abs} < F_a$, in which the delamination of the film from the substrate takes place. Near the lower threshold detachment of the film takes place at the time t_3 , approximately equal to 40 ps, see figure 4. Times t_1 and t_3 are approximately equal to 20 and 40 ps. They correspond to the first maximum of the positive contact pressure and the first minimum of negative contact pressure on figure 4. At time t_2 , approximately equal to 25 ps, the contact pressure passes through zero. Near threshold F_s detachment occurs at t_3 , since the negative pressure at this point, taken its absolute value, is the highest and equals to p_{coh} . Integral (1) taken from zero up to the time t_3 , is not equal to zero since the areas on the first half-period of the first half and the second half period are not equal. That is just above the threshold for delamination F_s film after the separation is flying at a finite speed.

Let's see how the value of p_{coh} affects to the velocity of the center of mass. Consider the calculation $F_{abs} = 30 \text{ mJ/cm}^2$ at tension of cohesion equal to zero p_{coh} and tension of cohesion equal to 1 GPa. Dependence of the time of contact pressure at 30 mJ/cm^2 is quite close to the same at 10 mJ/cm^2 if increasing the amplitude of figure 4 to about three times, and leaving the times $t_1 - t_3$ approximately the same. The separation of the film from the substrate at $p_{coh} = 0$ occurs at the time moment t_2 . Detachment occurs smoothly, without the formation of spall pulse as $p_{coh} = 0$. The speed of the center of mass in this case is 52 m/s. If $p_{coh} = -1 \text{ GPa}$, the separation takes place at a point on the time interval between times t_2 and t_3 . Moment of separation is closer to the point t_2 , and the velocity of the center of mass is reduced by 10% compared with the case of lack of cohesion $p_{coh} = 0$.

3.4. Ablation threshold and the internal breaking of the film

As mentioned above, depending on the energy F_{abs} there are three modes separated by thresholds F_s and F_a . The 1st and 2nd modes relating to the cases $F_{abs} < F_s$ and $F_s < F_{abs} < F_a$ were discussed above. Consider the remaining case: $F_a < F_{abs}$. Above the threshold of ablation film breaks in its middle part. Moreover, this occurs before the stretch zone of gold covers the whole film and reaches the contact "gold-glass". Figure 10 shows the case when absorbed energy is above the ablation threshold. In the film $F_{abs} = 40 \text{ mJ/cm}^2$. The initial stage of evolution is similar to the case with the $F_{abs} = 30 \text{ mJ/cm}^2$. From the edges of the film two waves propagate inside, the pressure in the middle being slowly rising (due to energy transfer from the electrons to the tighter ionic subsystem). At the time of 9 ps the head characteristics of these waves meet near the central plane of the film, the total pressure profile at the time of 9 ps $F_{abs} = 40 \text{ mJ/cm}^2$ being similar to the profile on figure 5 at the time of 10 ps for $F_{abs} = 30 \text{ mJ/cm}^2$. Maximum total (electronic plus ionic) pressure in the case of 40 mJ/cm^2 is 13 GPa, and in the case of 30 mJ/cm^2 is slightly higher than 8 GPa.

After the meeting in the center the rarefaction waves pass through each other and continue their further spread to the edges of the film. The pressure in the central zone begins to decline rapidly. See figure 10. The temperature of the film is above the melting point of gold. Low thermal conductivity of glass is neglected. Heating of the glass by a weak shock wave traveling through the glass being small. The initial temperature (before heating by the laser pulse) is 300 K. The temperature distribution is shown on figure 11. In gold the electron-ion temperature relaxation is slow. As you can see, even at the time of 15 ps there is a significant difference between electron and ion temperatures, see figure 11. Because of the large electron thermal conductivity and low film thickness, the electron temperature T_e is almost uniformly distributed over the gold film. Small irregularities in the distribution of the ion temperature T_i are associated with the following laser heating from the side of vacuum and the current instantaneous pressure distribution over the film. For example, the minimum temperature at $x = 40 \text{ nm}$ is situated in the point of minimum pressure, compare figures 10 and 11.

To describe the cavitation nucleation of stretched ($p < 0$) melt gold MD calculations were used, some of which are given in [13]. They calculated pressure (tensile stress) and the

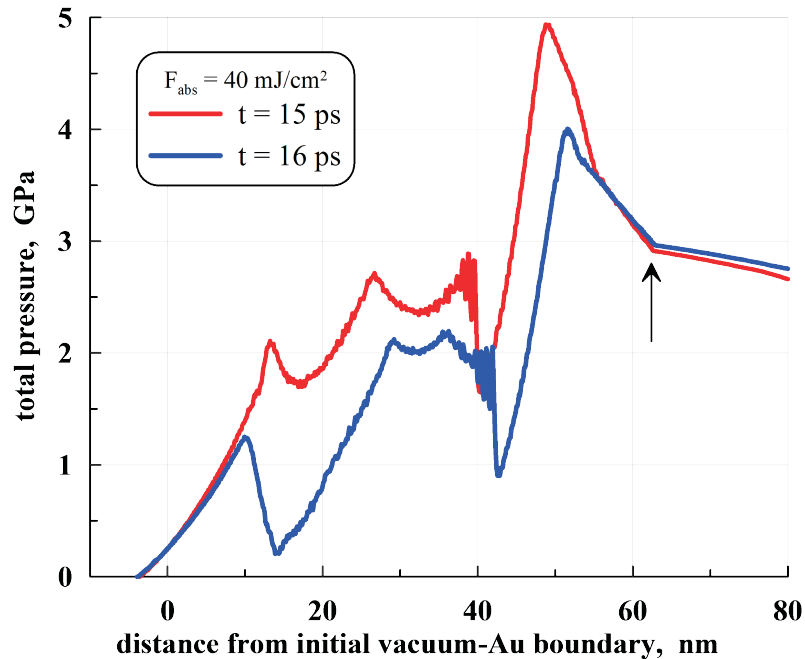


Figure 10. Rapid reduction in pressure after the meeting rarefaction waves in the center of the film at the time of 9 ps. The arrow marks the current position of the contact between the gold and the glass on the left to the right.

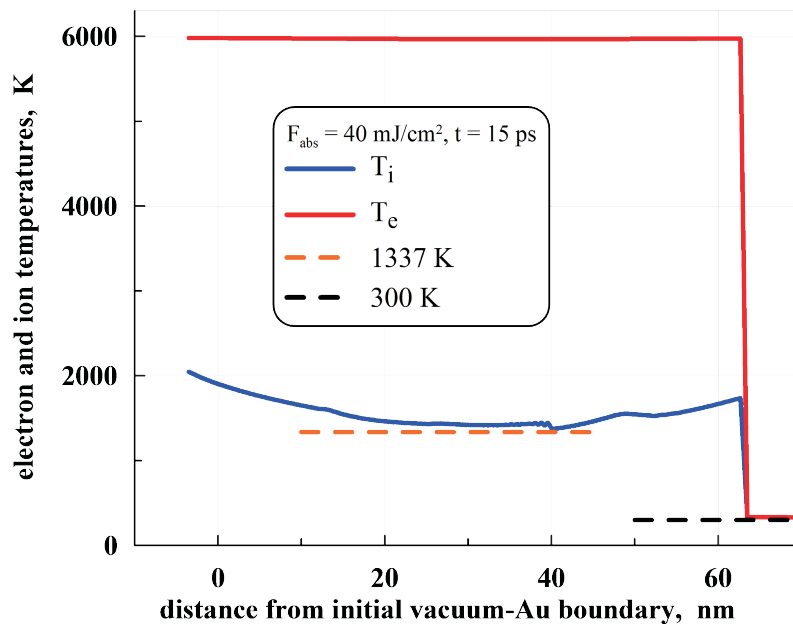


Figure 11. Distribution of ion and electron temperatures. Temperature jump right refers to the gold-glass contact.

temperature at the point of nucleation. It is known that the pressure at a constant temperature of nucleation depends on the time during which the sample is being under a given tensile stress, see [25] and references cited in this paper. They say that the pressure thermofluctuational

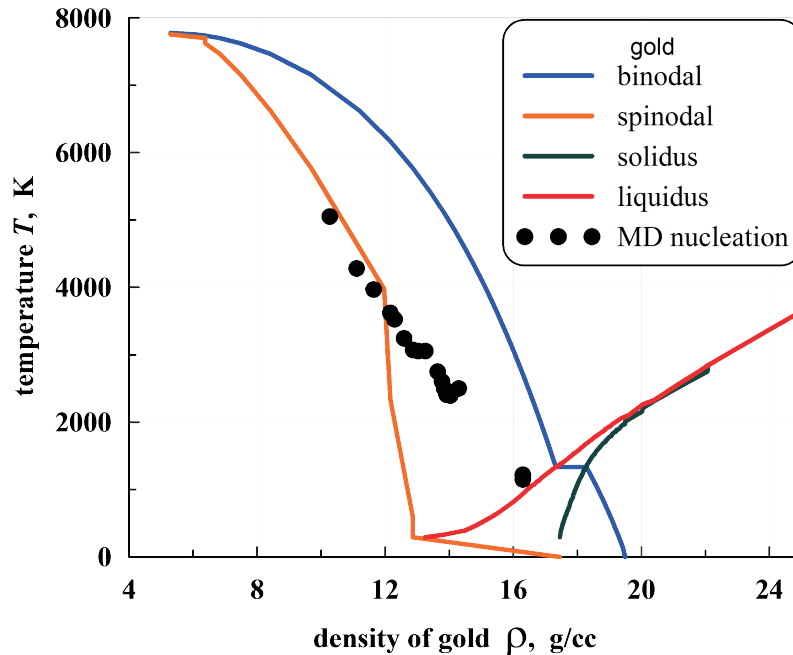


Figure 12. Pressure and temperature at which the nucleation takes place for film thickness of ~ 0.1 mm according to [13] (black circles).

nucleation depends on the rate of deformation V/\dot{V} : the more pace the more the amplitude of the tensile stress, which is required for the emergence of a viable fetus vapor. If the pressure and temperature in the nucleation point included in the exponential factor in the formula for the probability of nucleation, the rate of deformation is included in the pre-exponential factor. Therefore, the influence of the film thickness variation (the thinner the film, the higher V/\dot{V}) on the probability of nucleation is much weaker than the effect of pressure and temperature variations. However, in order to correctly calculate the probability in a problem on figures 12, 13, in the MD calculations the order of the film thickness was taken the same as in the problem of the internal rupture of the film. The temperature and density in the nucleation point in the case of stretching of the film with thickness of about 0.1 microns are shown as markers on figure 12, and the temperature and pressure are shown on figure 13. In MD calculations was used EAM potential of gold, developed by Zhakhovskii [22] according to data obtained by density functional theory. Figure 13 shows the approximating parabola:

$$p = -5.04 + 0.0017T - 1.49 \cdot 10^{-7} T^2, \quad (2)$$

with the temperature taken in K, and the pressure taken in GPa. This curve fits to the data of MD calculations. It is used in 2T-HD code for the determination of nucleation point.

Figure 14 shows the pressures distribution at the time of 16 ps. In contrast to figure 10, herein, beside the total pressure, are shown electronic and ionic pressure. Only a little energy remains in the electron subsystem to the 16 ps time moment, but still two-temperature relaxation is unfinished, see figure 11. Therefore, there is a considerable electron pressure. To discussion of issues related to electronic pressure is devoted the final part of section 3 above. We assume that the two-temperature conditions in the nucleation process are determined by the degree of stretching of the melt with respect to to the equilibrium density, which will be determined at a fixed ion temperature. The matter is that the ionic temperatures in consideration are relatively low in the sense that in the single-temperature conditions with such a temperature the electronic

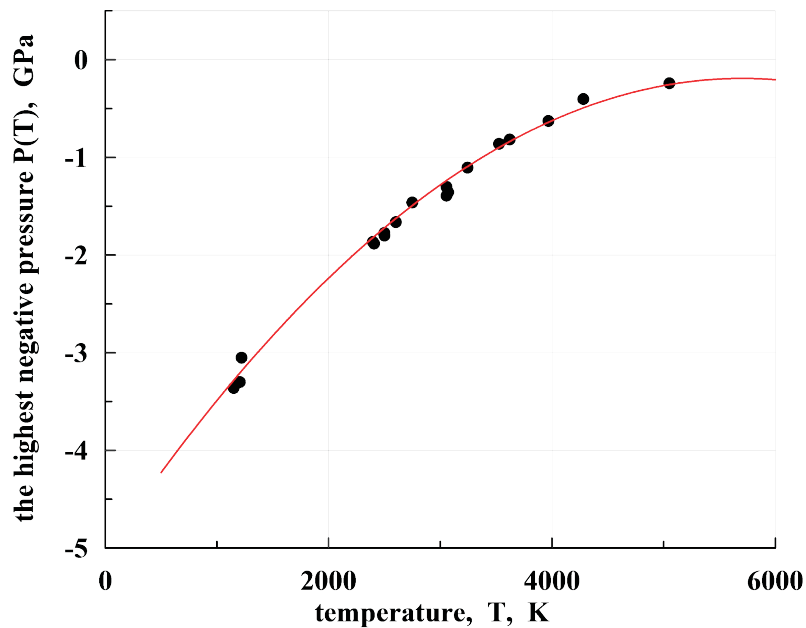


Figure 13. The temperature and pressure at which nucleation begins in gold.

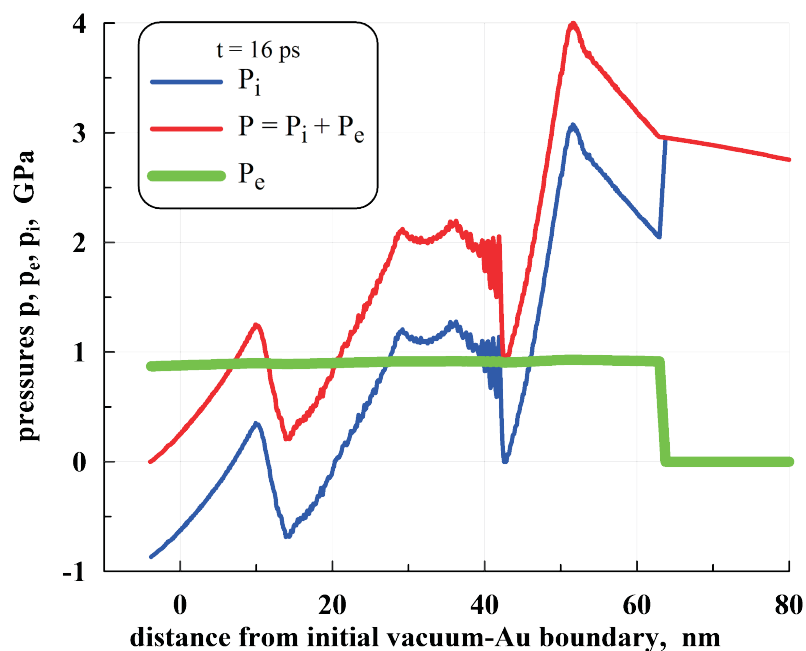


Figure 14. Pressure distribution. $F_{abs} = 40 \text{ mJ/cm}^2$. Electronic pressure further stretches the ionic subsystem.

contribution to the internal energy and the pressure is small. The electronic contribution becomes significant when the electronic temperature is much higher than the temperature of the ions. Therefore, a particular value of the degree of stretching is indicated by the pressure p_i in the ion subsystem. If the pressure p_i is positive, the system will be called compressed, otherwise we call it stretched.

At the time of 19.5 ps, the maximum tensile stress reaches a value that is determined by

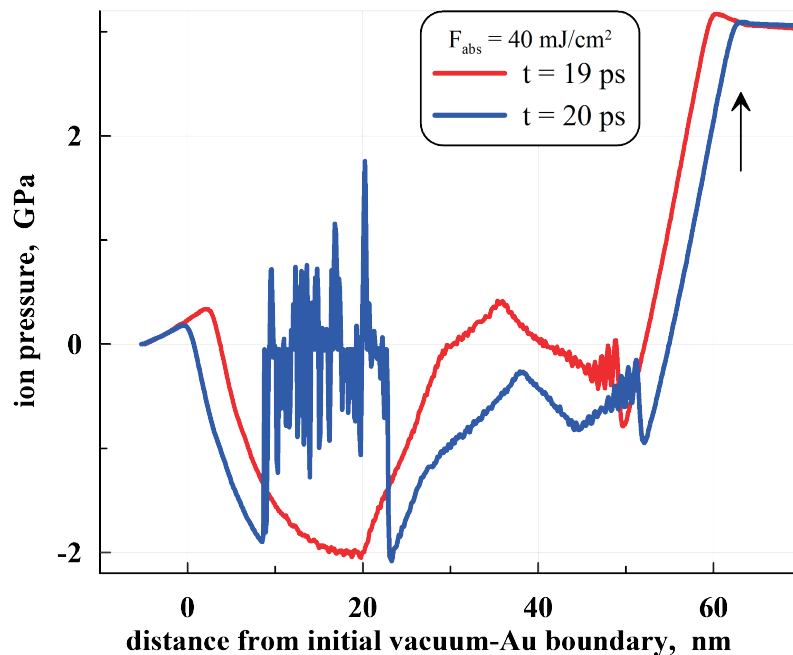


Figure 15. The evolution of the pressure profile of the ion momentum to rupture the film to the internal time after rupture. Contact position gold-glass at the time of 20 ps indicated by an arrow.

the formula (2). Nucleation and mechanical internal rupture of the film start. Pressure profiles at points 19 ps and 20 ps are shown on figure 15. By 20 ps gap covers a significant layer thickness of 9 nm to 23 nm. Recall that before laser exposure to the substance of the film took a segment from 0 to 60 nm. Ion pressure profile $p(x, t)$ at the time of 20 ps on the range of $9 \text{ nm} < x < 23 \text{ nm}$ greatly fluctuates near zero, see. figure 15. At the time of 20 ps, the first characteristic of the rarefaction wave that runs from left to right on the border with vacuum reaches the contact with the glass, compare figures 10, 14, 15. The pressure at the contact point remains positive at the moment of the internal gap of the film and for a short while after.

4. Conclusion

We consider the problem with a small spot on the thin film. It is shown that in the case of experimental interest [15–17] film separated from the substrate and forms a swelling on the substrate. An explanation of the vibrational motion and delamination of the film is given. Apparently first described three modes of motion of the film on the substrate film after irradiation by femtosecond impulse. These are vibrational mode, delamination mode and internal rupture mode.

Acknowledgments

Support from RFBR grant No.13-08-01095 and RAS program “Substance at high energy densities” is acknowledged. V V Shepelev performed two-temperature hydrodynamic by a grant from the Russian Science Foundation No.14-11-00719. Molecular dynamics simulations were performed on a supercomputer “Lomonosov” Moscow State University.

References

- [1] Ashitkov S I, Inogamov N A, Zhakhovskii V V, Emirov Y N, Agranat M B, Oleinik I I, Anisimov S I and Fortov V E 2012 *JETP Letters* **95** 176–181

- [2] Inogamov N A, Zhakhovsky V V, Khokhlov V A, Ashitkov S I, Emirov Y N, Khichshenko K V, Faenov A Y, Pikuz T A, Ishino M, Kando M, Hasegawa N, Nishikino M, Komarov P S, Demaske B J, Agranat M B, Anisimov S I, Kawachi T and Oleynik I I 2014 *J. Phys.: Conf. Series* **510** 012041–1–012041–15
- [3] Wu C and Zhigilei L V 2014 *Applied Physics A* **114** 11–32
- [4] Zhakhovskii V V and Inogamov N A 2010 *JETP Letters* **92** 521–526
- [5] Ashitkov S I, Agranat M B, Kanel' G I, Komarov P S and Fortov V E 2010 *JETP Letters* **92** 516–520
- [6] Sokolowski-Tinten K, Bialkowski J, Cavalleri A, von der Linde D, Oparin A, ter Vehn J M and Anisimov S 1998 *Phys. Rev. Lett.* **81** 224–227
- [7] Inogamov N A, Petrov Y V, Anisimov S I, Oparin A M, Shaposhnikov N V, von der Linde D and Meyer-ter Vehn J 1999 *JETP Letters* **69** 310–316
- [8] Zhakhovskii V V, Nishihara K, Anisimov S I and Inogamov N A 2000 *JETP Letters* **71** 167–172
- [9] Anisimov S I, Zhakhovskii V V, Inogamov N A, Nishihara K, Oparin A M and Petrov Y V 2003 *JETP Letters* **77** 606–610
- [10] Anisimov S I, Zhakhovskii V V, Inogamov N A, Nishihara K and Petrov Y V 2007 *Applied Surface Science* **253** 6390–6393
- [11] Povarnitsyn M E, Itina T E, Sentis M, Khishchenko K V and Levashov P R 2007 *Physical Review B* **75** 235414
- [12] Upadhyay A K, Inogamov N A, Rethfeld B and Urbassek H M 2008 *Physical Review B* **78** 045437
- [13] Demaske B J, Zhakhovsky V V, Inogamov N A and Oleynik I I 2010 *Physical Review B* **82** 064113
- [14] Leguay P M, Levy A, Chimier B, Deneuville F, Descamps D, Fourment C, Goyon C, Hulin S, Petit S, Peyrusse O, Santos J J, Combis P, Holst B, Recoules V, Renaudin P, Videau L and Dorchies F 2013 *Phys. Rev. Lett.* **111**
- [15] Unger C, Koch J, Overmeyer L and Chichkov B N 2012 *Optics Express* **20** 24864
- [16] Nakata Y, Tsuchida K, Miyanaga N and Okada T 2008 *Journal of Laser Micro/Nanoengineering* **3** 63–66
- [17] Emelyanov V I, Zayarniy D A, Ionin A A, Kiseleva I V, Kudryashov S I, Makarov S V, Nguyen T H T and Rudenko A A 2014 *JETP Letters* **99** 518–522
- [18] Levashov P R and Khishchenko K V 2007 *AIP Conf. Proc.* **955** 59–62
- [19] Khishchenko K V 2008 *J. Phys.: Conf. Series* **98** 032023
- [20] Khishchenko K V 2008 *J. Phys.: Conf. Series* **121** 022025
- [21] Khishchenko K V 2015 *J. Phys.: Conf. Series* This issue (*Preprint arXiv:1510.00763*)
- [22] Zhakhovskii V V, Inogamov N A, Petrov Y V, Ashitkov S I and Nishihara K 2009 *Applied Surface Science* **255** 9592–9596
- [23] Inogamov N A and Zhakhovskii V V 2014 *JETP Letters* **100** 4–10
- [24] Petrov Y V, Migdal K, Inogamov N A and Zhakhovsky V V *Applied Physics B: Lasers and optics (sent to journal)*
- [25] Ashitkov S I, Komarov P S, Ovchinnikov A V, Struleva E V, Zhakhovskii V V, Inogamov N A and Agranat M B 2014 *Quantum Electronics* **44** 535–539